metals

MDPI

Article

Study on the Wear Resistance of Laser-Cladded CoCrFeMnNi Coatings Under Machine Hammer Peening

Rui Wang [1,2], Juan Hou [1], Lu Yu [1], Shouwei Xu [1], Lihong Su [2], Hui Wang [1,3] and Xi Huang [1,*]

[1] School of Mechanical Engineering, Nantong University, Nantong 226019, China; rui_wang@uow.edu.au (R.W.); 2310110192@stmail.ntu.edu.cn (J.H.); 2310110003@stmail.ntu.edu.cn (L.Y.); 2310110228@stmail.ntu.edu.cn (S.X.); hui_wang@metall.t.u-tokyo.ac.jp (H.W.)
[2] School of Mechanical, Materials, Mechatronic and Biomedical Engineering, University of Wollongong, Wollongong, NSW 2522, Australia; lihongsu@uow.edu.au
[3] Institute for Industrial Science, The University of Tokyo, Chiba 153-8505, Japan
* Correspondence: huangxi@ntu.edu.cn

Abstract

CoCrFeMnNi high-entropy alloy (HEA) coatings were fabricated on an S41500 stainless steel substrate by laser cladding and subsequently strengthened using machine hammer peening (MHP) at three hammering energies of 1.7 J, 3.5 J, and 5.0 J. The effects of MHP treatment on the phase structure, surface morphology, microhardness, and tribological properties of the coatings were systematically investigated. The results showed that all coatings retained a single-phase face-centered cubic (FCC) structure after MHP treatment, indicating excellent microstructural stability during impact-induced strengthening. With increasing hammering energy, the surface morphology gradually evolved from discrete hammering indentations to a more continuous orange-peel-like texture, while the surface roughness initially increased and then decreased. MHP significantly enhanced the surface hardness of the coatings. In particular, the MHP3.5 sample exhibited the highest surface hardness of approximately 420 HV, representing an increase of about 120% compared with the untreated coating. Under dry sliding conditions at a load of 30 N, the MHP3.5 sample exhibited the lowest and most stable friction coefficient, maintaining a steady-state value of approximately 0.40–0.45. Its specific wear rate decreased by nearly 45% compared with that of the untreated coating. The improved wear resistance was mainly attributed to the combined effects of strain hardening, grain refinement, and dislocation strengthening induced by machine hammer peening. Considering the hardness, friction coefficient, and specific wear rate results together, a hammering energy of 3.5 J was identified as the most suitable MHP parameter under the low-load wear conditions investigated in this study.

Keywords: CoCrFeMnNi coating; laser cladding; machine hammer peening; microhardness; wear resistance

Check for updates

Academic Editor: Slobodan Mitrovic

Received: 9 June 2026
Revised: 24 June 2026
Accepted: 26 June 2026
Published: 29 June 2026

Copyright: © 2026 by the authors. Licensee MDPI, Basel, Switzerland. This article is an open access article distributed under the terms and conditions of the Creative Commons Attribution (CC BY) license.

1. Introduction

In modern industrial systems, critical components such as hydraulic machinery blades and marine sliding parts are frequently exposed to severe friction, impact, and corrosive service environments [1–3]. Surface degradation caused by wear not only reduces the dimensional accuracy and service life of these components but also threatens the operational safety of the whole equipment system [2]. Conventional surface modification or repair methods, including electroplating, thermal spraying, and surfacing, still suffer from limitations such as weak interfacial bonding, environmental concerns, or insufficient long-term

wear resistance [4]. Laser cladding has therefore attracted increasing attention because it can metallurgically bond a functional coating to the substrate and repair high-value components with relatively low thermal distortion [5]. However, as-cladded coatings generally contain solidification microstructures, surface undulations, residual stresses, and limited surface hardness, which may restrict their tribological performance under severe sliding conditions.

High-entropy alloys (HEAs) provide a promising class of coating materials because of their high configurational entropy, sluggish diffusion effect, severe lattice distortion, and cocktail effect [6–9]. These characteristics allow HEAs to exhibit attractive combinations of strength, toughness, corrosion resistance, and wear resistance compared with many conventional alloys [10–13]. Among various HEAs, equiatomic CoCrFeMnNi, also known as the Cantor alloy, is one of the most representative single-phase face-centered cubic (FCC) systems. The selection of CoCrFeMnNi in this work is not only based on its wide use as a model HEA, but also on its intrinsic suitability for surface strengthening and tribological applications. Its FCC matrix provides good ductility, multiple slip systems, and strong work-hardening capability, allowing the material to accommodate severe plastic deformation without premature brittle cracking [14–16]. Moreover, previous studies have shown that CoCrFeMnNi can exhibit stable sliding wear behavior, which is associated with friction-induced grain refinement and the lubricating effect of oxide wear debris [17,18].

Nevertheless, CoCrFeMnNi also has an important limitation: its initial hardness and yield strength at room temperature are relatively low compared with many hard coating systems [17–19]. This feature is a double-edged sword. On the one hand, the low hardness may reduce the resistance of the coating to abrasive plowing and material removal during sliding wear. On the other hand, the excellent plastic deformability of the FCC matrix makes CoCrFeMnNi particularly suitable for post-cladding mechanical surface strengthening. Therefore, an effective strategy is to first fabricate a dense and metallurgically bonded CoCrFeMnNi coating by laser cladding and then introduce a surface deformation treatment to improve the near-surface hardness and wear resistance.

Machine hammer peening (MHP) is a non-thermal surface strengthening technique that produces repeated high-frequency impacts on the material surface [20–22]. During MHP, severe plastic deformation can be introduced into the near-surface layer, resulting in grain refinement, dislocation accumulation, subgrain formation, and residual compressive stress. These microstructural and stress-state modifications are beneficial for improving surface hardness, suppressing abrasive cutting, and enhancing wear resistance [23–25]. Compared with surface treatments that rely mainly on heating, coating deposition, or phase transformation, MHP is especially suitable for FCC CoCrFeMnNi coatings because the FCC matrix can accommodate impact-induced plastic strain and transform it into work hardening rather than brittle damage.

Although laser-cladded HEA coatings have been widely studied in terms of alloy composition, cladding parameters, phase constitution, and tribological behavior, most existing studies focus on the as-cladded state. The post-cladding mechanical strengthening of laser-cladded FCC HEA coatings remains insufficiently understood. In addition, previous MHP studies have mainly concentrated on conventional alloys, welded joints, additively manufactured metals, or traditional coating systems. Their conclusions cannot be directly transferred to laser-cladded CoCrFeMnNi HEA coatings, because such coatings possess unique solidification structures, metallurgical bonding interfaces, dilution behavior, residual stress states, and FCC-dominated deformation mechanisms. Therefore, it is still unclear how hammering energy affects the surface integrity and wear response of laser-cladded CoCrFeMnNi coatings.

Based on this consideration, the present study investigates the effect of different machine hammer peening energies on the surface characteristics and wear resistance of laser-cladded CoCrFeMnNi HEA coatings. The coating was first prepared using optimized laser cladding parameters and then subjected to different hammering energies. The phase constitution, surface morphology, roughness, microhardness gradient, friction coefficient, specific wear rate, and worn surface morphology were systematically analyzed. The novelty of this work lies in revealing the hammering-energy-dependent strengthening response of a laser-cladded single-phase FCC CoCrFeMnNi coating. In particular, this study aims to clarify whether a suitable MHP energy window exists, in which sufficient plastic deformation can improve surface hardness and wear resistance, whereas insufficient or excessive hammering energy may fail to produce the optimal tribological response.

2. Experimental Materials and Methods

2.1. Experimental Materials and Equipment

S41500 stainless steel with dimensions of 40 × 40 × 20 mm^3 was used as the substrate. The coating material was CoCrFeMnNi high-entropy alloy pre-alloyed powder prepared by gas atomization, with nearly equiatomic atomic percentages of all elements and a purity of 99.99%.

2.2. Process Parameters

Before laser cladding, samples were pre-treated by surface grinding and cleaning. The substrate surface was sequentially polished using sandpapers of varying grit to remove oxides and contaminants, followed by ultrasonic cleaning with 98% ethanol and drying. Argon (99.999 wt%) was used as the shielding gas at a flow rate of 25 mL/min to prevent oxidation during cladding. The basic laser cladding parameters were laser spot diameter of 4 mm, scanning speed of 16 mm/s, focal length of 150 mm, 40% overlap between adjacent tracks, laser power of 3500 W, and a target coating thickness of approximately 1 mm.

Prior to machine hammer peening, samples were securely fixed, ensuring no displacement during peening. The hammering was performed in a point-by-point reciprocating mode along a predefined path on the coating surface. To study the effect of hammering energy on coating performance, three energy levels were selected for comparison: 1.7 J, 3.5 J, and 5.0 J, representing low, medium, and high energy densities, respectively. Sample labeling was as follows: unpeened sample as MHP0, and peened samples as MHP1.7, MHP3.5, and MHP5.

2.3. Structural and Microstructural Characterization

2.3.1. X-Ray Diffraction (XRD) Analysis

The phase structure of the coatings under different treatments was characterized using an Ultima IV X-ray diffractometer (Rigaku Corporation, Tokyo, Japan) at room temperature (25 ± 2 °C) and standard atmospheric pressure, employing a Cu Kα target. The operating voltage and current were 40 kV and 30 mA, respectively. The scanning range was 5–100°, with a step size of 0.02°, 1 s per step, and a scanning rate of 4°/min. This analysis aimed to determine whether machine hammer peening induced phase transformation or secondary phase precipitation, evaluating the structural stability of the high-entropy alloy under strong impact. The positions, intensities, and shapes of diffraction peaks were analyzed to determine phase composition, lattice constants, and grain orientation.

2.3.2. Surface Morphology

A combination of extended-depth-of-field microscopy and laser confocal scanning microscopy was used to evaluate the surface quality of coatings before and after machine

hammer peening at multiple scales. Extended-depth-of-field microscopy observed the macroscopic evolution of the coating from the original sprayed state to the peened state. Confocal microscopy captured three-dimensional microstructural images, and key roughness parameters, such as the arithmetic average height, were quantitatively extracted to assess the improvement in surface flatness under different hammering energies, elucidating the influence of surface geometry evolution on subsequent frictional wear. Additionally, field-emission scanning electron microscopy (FE-SEM, Zeiss Sigma 300(Carl Zeiss AG, Oberkochen, Germany)) was employed to characterize the microstructure of the worn coating surface at 15 kV, allowing detailed observation of wear tracks, pits, interlayer gaps, and microcracks to investigate the transformation of wear mechanisms under various hammering energies.

2.4. Mechanical and Tribological Performance Testing

2.4.1. Microhardness Testing

The microhardness distribution of the coating cross-section was measured using an HV-1000 Vickers hardness tester(Laryee Technology Co., Ltd., Jinan, China) under a 200 g load with a 15 s dwell time. Measurements were taken every 50 μm from the coating surface to the substrate. After hammer peening, the surface hardness increased significantly; hence, a 1000 g load was used, with test points forming standard rhombic indentations with diagonal lengths of 40–70 μm. A staggered measurement method was applied to prevent interference between adjacent points as Figure 1. Each condition was tested three times to ensure reliability, and the average value was reported.

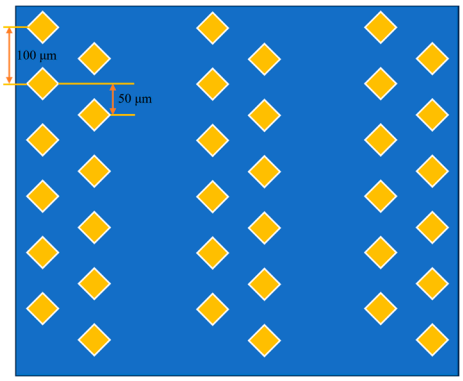


Figure 1. Microhardness testing schematic.

2.4.2. Friction and Wear Testing

Wear tests under dry friction conditions were performed using an MFT-5000 tribometer (Rtec Instruments Inc., San Jose, CA, USA). A 6 mm diameter SiC pin was used as the counterface, with a reciprocating frequency of 1 Hz and a single sliding distance of 9 mm. The total test duration was set to 600 s, corresponding to 600 cycles, which resulted in a total sliding distance of 10.8 m (calculated as 9 mm × 2 × 1 Hz × 600 s). After hammer peening, the coating surface was significantly strengthened; to ensure clear scratch patterns for analysis, a load of 30 N was applied, and both friction coefficients and wear rates were recorded. It should be noted that the present dry sliding wear test was not intended to directly simulate the corrosion or cavitation conditions encountered by hydraulic components in service. A hard SiC pin was employed as the counterbody to specifically characterize the mechanical wear behavior of the coating under solid contact, repeated ploughing, and cyclic loading conditions, thereby minimizing the influence of factors such as liquid-phase chemical reactions and cavitation impacts on the evaluation of the machine hammer peening strengthening effect. Therefore, the friction coefficient, specific wear

rate, and worn surface morphology obtained in this study were used solely to assess the mechanical wear resistance of the coating. Prior to wear testing, the initial coatings were prepared by standard metallographic procedures: sequential grinding with 400–2000 grit SiC papers, polishing with 3 μm and 1 μm diamond suspensions, and final polishing with 0.04 μm SiO_2 suspension. Surface roughness was controlled below Ra < 0.1 μm to eliminate the influence of initial surface state. Hammer-peened coatings were tested directly without metallographic preparation to reflect the strengthening effect. After each test, mass loss was measured using a 0.1 mg precision balance (YTL1204) (Zhejiang Yongtailong Electronic Co., Ltd., Tongxiang, China). Each condition was tested three times to ensure reliability.

After the wear tests, the mass loss of each sample was determined using an electronic balance with an accuracy of 0.1 mg. The specific wear rate was then calculated based on the measured mass loss. The specific wear rate was calculated according to:

$$W = \frac{\Delta V}{F \times L} = \frac{\Delta m}{\rho \times F \times L}$$

where W is the specific wear rate ($mm^3 \cdot N^{-1} \cdot m^{-1}$), ΔV is the wear volume loss (mm^3), Δm is the mass loss before and after wear testing (g), ρ is the coating density ($g \cdot mm^{-3}$), F is the applied normal load (30 N in this study), and L is the total sliding distance (m). The total sliding distance was calculated from the reciprocating sliding stroke length, sliding frequency, and test duration. To ensure the reliability of the results, each wear test was repeated three times, and the average value was reported as the final result.

3. Results and Analysis

3.1. Coating Analysis

3.1.1. XRD Phase Analysis of Coatings

The XRD patterns of coatings subjected to different hammering energies (MHP1.7, MHP3.5, and MHP5) are shown in Figure 2. All samples exhibit typical single-phase face-centered cubic (FCC) characteristics corresponding to (111), (200), (220), and (311) planes, with no obvious oxide or secondary phase peaks detected. This indicates that hammering energy does not alter the phase composition of the coating, and the alloy maintains good structural stability. It should be noted that the weak diffraction peak observed near 96° can be indexed to the FCC (222) crystal plane, further confirming that the coating retained a face-centered cubic structure after machine Hammer Peening treatment. A weak signal can also be observed near 28°; however, this peak does not correspond to a major characteristic diffraction peak of the FCC CoCrFeMnNi high-entropy alloy matrix. It may be associated with a small amount of surface oxides, background noise, or local impurities. Because the intensity of this weak peak is relatively low and does not exhibit a systematic increase with increasing hammering energy, it is reasonable to conclude that machine hammer peening at different energy levels did not significantly alter the primary phase constitution of the coating. The coating therefore remained predominantly composed of a single FCC phase after MHP treatment.

With increasing hammering energy, the diffraction peak intensities and shapes change significantly. Compared to MHP1.7, MHP3.5 and MHP5 show enhanced peak intensities, sharper peak shapes, and reduced half-widths These changes suggest that MHP treatment induced crystallographic orientation rearrangement in the surface layer and enhanced the preferential orientation tendency of the FCC(111) plane. Previous studies on machine hammer peening, shot peening, and ultrasonic impact treatment have shown that repeated impact loading can induce severe plastic deformation in the near-surface region, leading to grain rotation, dislocation slip, and crystallographic reorientation. These microstructural changes are often reflected in XRD patterns through variations in relative peak intensity,

peak shape, and peak broadening. The present results are consistent with these reported mechanisms, indicating that MHP treatment altered the crystallographic orientation state of the surface grains while maintaining the single-phase FCC structure of the CoCrFeMnNi coating [20–25]. In addition, higher hammering energies may promote further plastic rearrangement of the surface layer, resulting in a denser surface microstructure and reduced diffraction background fluctuations associated with cladding defects and lattice distortion, thereby improving peak definition. Moreover, the relative intensity ratio between FCC(111) and FCC(200) peaks varies among samples. In MHP5, FCC(111) is most prominent, while in MHP1.7, (111) and (200) peaks have similar intensities. This suggests that higher hammering energy induces preferential grain orientation, promoting (111) plane growth, reflecting stronger plastic deformation and dislocation activity, resulting in a denser and more uniform surface microstructure. Overall, appropriate hammering energy improves crystal quality and surface stability.

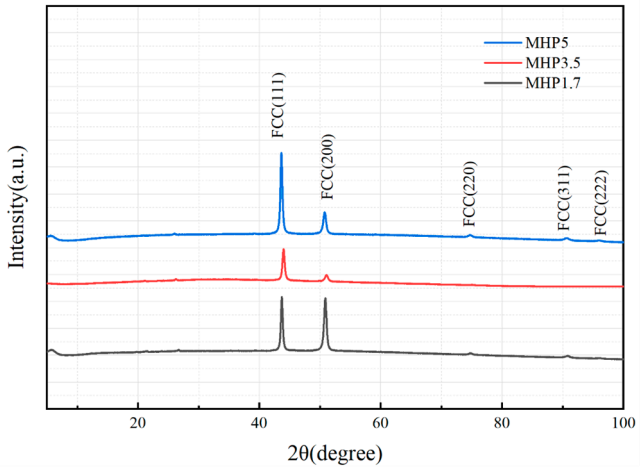


Figure 2. XRD Patterns of MHP1.7, MHP3.5, and MHP5.

3.1.2. Surface Morphology Analysis

The evolution of surface morphology of CoCrFeMnNi high-entropy alloy coatings under different hammering energies is shown in Figures 3 and 4. These figures are used to analyze the effects of hammering energy on surface plastic deformation, the merging of hammering-induced indentations, and the resulting changes in surface roughness. With increasing energy, the surface undergoes systematic changes: MHP1.7 exhibits relatively discrete and irregular hammer pits (Ra = 3.44 μm) with shallow depth and clear boundaries, indicating limited localized plastic deformation under low energy. MHP3.5 shows partially fused hammer marks with weakened boundaries (Ra = 4.22 μm), forming extensive undulations with localized material accumulation and plastic flow, reflecting broader surface plastic rearrangement under medium energy, yet still non-uniform. MHP5 displays fine and uniform "orange-peel" texture (Ra = 3.03 μm) with nearly invisible boundaries, a smoother overall undulation, highly continuous and uniform surface, and improved gloss consistency.

The surface roughness exhibits a nonlinear relationship with hammering energy, initially increasing and then decreasing. Medium energy results in local material accumulation and uneven plastic deformation, producing peak roughness, whereas high energy promotes uniform material flow, eliminating discrete boundaries and creating a smoother, continuous surface. This transition from discrete pits to continuous orange-peel texture reflects changes in the extent and mode of plastic deformation: low energy produces localized deformation, medium energy results in uneven large-area flow, and high energy achieves uniform surface rearrangement. Differences in surface roughness directly affect service

performance, and the uniform orange-peel surface of MHP5 favors excellent frictional stability during wear tests.

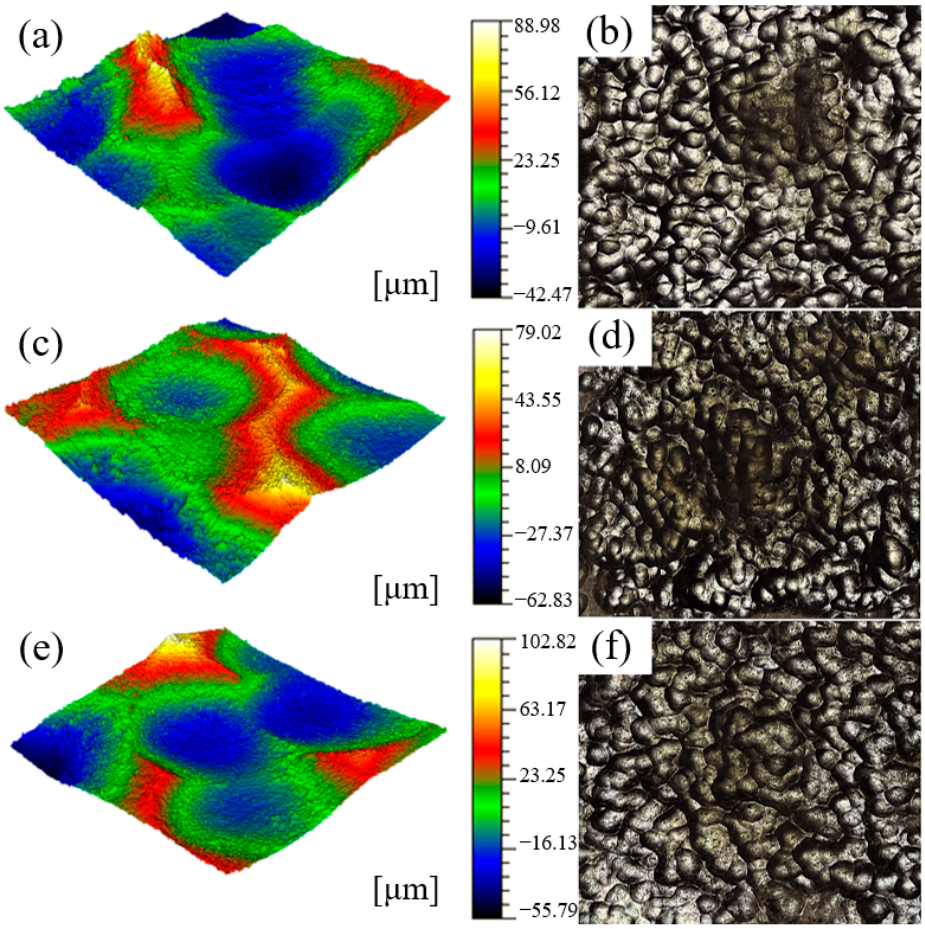


Figure 3. Hammered surface morphology of high-entropy alloy coatings: (**a**,**b**) MHP1.7, (**c**,**d**) MHP3.5, and (**e**,**f**) MHP5.

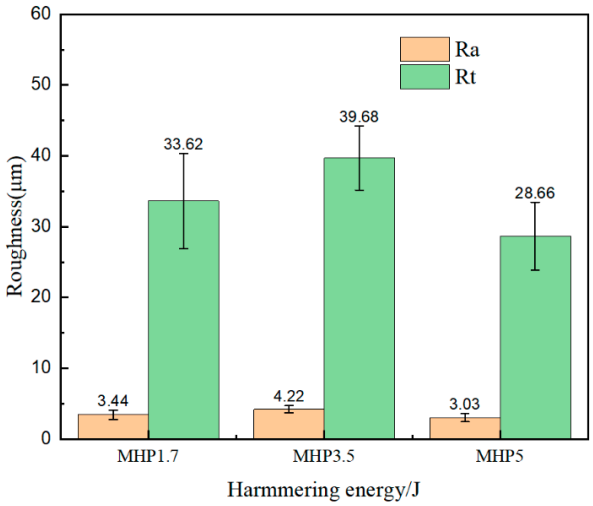


Figure 4. Surface roughness of different samples.

3.2. Coating Microhardness Analysis

To investigate the effect of machine hammer peening (MHP) on the mechanical properties of laser-cladded CoCrFeMnNi high-entropy alloy coatings, microhardness tests were systematically conducted on the unpeened sample (MHP0) and samples treated with three

different hammering energies (MHP1.7, MHP3.5, and MHP5.0). The hardness distribution from the coating surface to a depth of 1200 μm is shown in Figure 5.

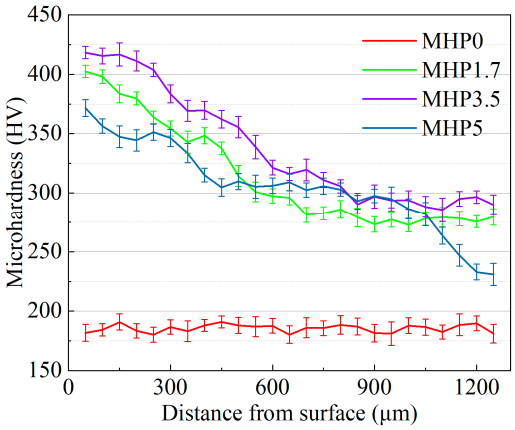


Figure 5. Microhardness of MHP0, MHP1.7, MHP3.5, and MHP5.

The MHP0 sample maintains a hardness of 180–190 HV throughout the tested depth, showing no significant depth dependence. This uniform hardness distribution corresponds to the homogeneous FCC single-phase structure formed during laser cladding, reflecting the stability of the as-cladded microstructure.

All hammer-peened samples exhibit a pronounced hardness gradient. The strengthening effect induced by MHP can be divided into three characteristic regions according to the hardness distribution: a primary strengthening region (0–300 μm), a transition region (300–900 μm), and a weakly affected deep region beyond 900 μm. In the surface region (0–300 μm), hardness significantly increases and gradually decreases with depth. MHP3.5 shows the highest surface hardness at approximately 420 HV, an increase of about 120% compared to MHP0. MHP1.7 has a surface hardness around 400 HV (+110%), while MHP5.0 reaches approximately 370 HV (+95%). The enhanced surface hardness results from several strengthening mechanisms induced by machine hammer peening. Among them, strain hardening caused by severe plastic deformation is considered the dominant strengthening mechanism. During hammer peening, a high density of dislocations is generated and accumulated in the near-surface region, resulting in significant work hardening. In addition, severe impact deformation is widely reported to induce grain refinement and the formation of nanoscale structures. According to the Hall–Petch relationship, such potential microstructural refinement, along with high-density dislocation boundaries, would contribute to the observed hardness enhancement. Furthermore, dislocation boundaries, subgrain boundaries, and residual compressive stresses generated during hammer peening provide additional strengthening effects. Similar strengthening mechanisms have also been reported in machine hammer peened titanium alloys and other metallic materials [20,26]. In the intermediate transition zone (300–900 μm), the hardness differences among the hammer-peened samples gradually decrease but remain higher than MHP0. This region can be regarded as a transition layer where the strengthening effect progressively attenuates with increasing depth while still maintaining a noticeable hardness advantage over the untreated coating. This indicates that the strengthening effect of hammer peening extends beyond the surface. MHP3.5 maintains relatively high hardness in this region, confirming the superior deep-layer strengthening effect of medium-energy hammering.

Beyond 900 μm depth, MHP5.0 exhibits a significant hardness drop, reaching approximately 230 HV at 1200 μm, lower than other peened samples. This deep layer hardness degradation is probably correlated with the inhomogeneous distribution of the deformation layer, variations in local work-hardening degrees, and the attenuation of strengthening

effects within the deep microstructure under high-energy hammering. In contrast, MHP3.5 and MHP1.7 maintain around 280–300 HV in the deep region, indicating more stable and lasting strengthening under medium and low energy.

In summary, MHP3.5 exhibits the optimal hardness increase both at the surface and in deeper layers, providing a mechanical foundation for superior wear performance under subsequent 30 N loading.

3.3. Friction and Wear Performance Analysis

3.3.1. Specific Wear Rate

Machine hammer peening significantly affects the wear resistance of coatings and exhibits load dependence. Figure 6 presents a comparison of the specific wear rates of MHP0 and the coatings treated with different hammering energies under a load of 30 N.

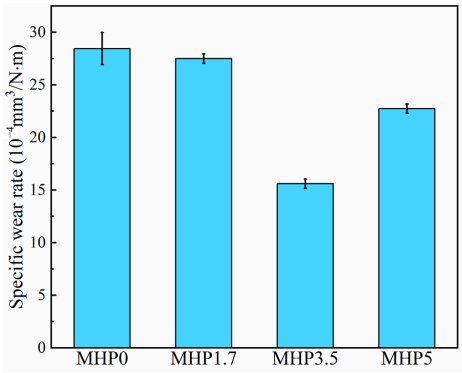


Figure 6. Specific wear rates of MHP0, MHP1.7, MHP3.5, and MHP5 under 30 N load.

As can be observed, MHP0 exhibits the highest specific wear rate under this load, indicating the poorest wear resistance. Following the machine hammer peening treatment, the specific wear rates of all coatings decrease to varying degrees, resulting in a substantial enhancement of their wear performance. Specifically, the MHP3.5 sample treated with medium hammering energy displays the optimal performance, achieving a reduction of nearly 45% and demonstrating outstanding wear resistance under low-load conditions. In contrast, the MHP1.7 sample subjected to low-energy hammering shows a limited decrease in the specific wear rate compared to MHP0, which suggests that the strengthening effect of low-energy hammering is relatively weak. Although the MHP5 sample processed with high-energy hammering outperforms MHP0 and MHP1.7 in terms of wear resistance, its performance remains slightly inferior to that of MHP3.5.

This indicates that under low-load conditions, medium-energy hammering is expected to induce a favorable combination of grain refinement and dislocation density, most effectively resisting abrasive cutting and achieving optimal wear performance, while excessive or insufficient energy cannot attain the best low-load wear strengthening effect.

3.3.2. Friction Coefficient Analysis

Figure 7 shows the friction coefficient-time curves of CoCrFeMnNi high-entropy alloy coatings treated with different hammering energies under a 30 N load. Comparative analysis clearly reveals the influence of machine hammer peening on the friction behavior of the coatings.

MHP0 exhibits significant instability. In the initial stage (0–100 s), the friction coefficient fluctuates violently between 0.25 and 0.6, then gradually rises and stabilizes at a high level of 0.55–0.60. This is closely related to the coarse-grain structure of the as-cladded coating, high surface roughness, and the predominance of abrasive wear. On one hand, the laser-cladded coating contains coarse dendritic structures, numerous pores and inclusions,

and high roughness, making the contact interface prone to alternating "plowing–adhesion" actions, causing initial severe fluctuations. On the other hand, the original low hardness allows SiC micro-protrusions to easily penetrate and remove material, while the generated debris further intensifies abrasive wear, maintaining a high friction coefficient. In contrast, the initial fluctuation ranges of all hammer-peened samples are significantly narrowed, indicating that the high hardness of the strengthened layer effectively suppresses severe initial plowing, allowing the friction pair to reach a stable state more quickly.

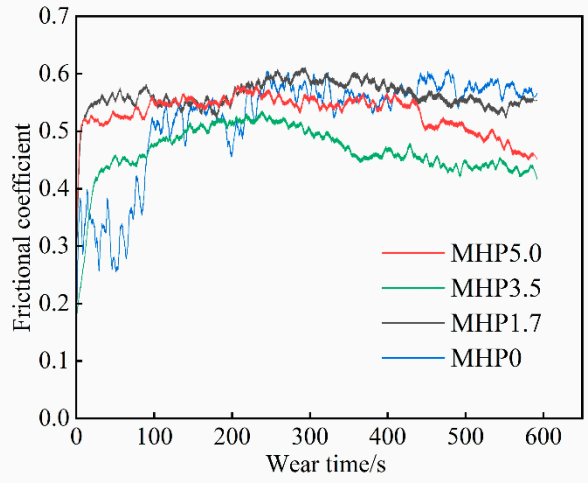


Figure 7. Friction coefficient-time curves under a 30 N load.

After machine hammer peening, the friction behavior of the coatings shows clear differences.

MHP3.5 exhibits the lowest and most stable friction coefficient. After a rapid initial increase, it remains steady at 0.40–0.45 with minimal fluctuation. This behavior can be attributed to the more pronounced work-hardening effect induced by medium-energy hammer peening, which produced higher surface hardness and a more stable load-bearing state in the near-surface region of the coating. The significantly enhanced surface hardness effectively resisting abrasive plowing, while moderate dislocation density provides plastic deformation capability, promoting the formation of a continuous and stable friction interface, resulting in optimal friction reduction.

The friction coefficient of MHP5.0 is slightly higher than that of MHP3.5, stabilizing at 0.50–0.55, but shows a slow decrease in the later stage (500–600 s). High-energy hammer peening induced more pronounced plastic deformation in the coating surface layer and produced a more complex surface topography. During the initial stage of sliding, the higher hammering energy may have resulted in a non-uniform distribution of plastic strain, defect density, and residual stress within the surface layer. Consequently, some surface asperities could not be fully smoothed through coordinated plastic deformation, leading to a relatively stronger ploughing effect at the contact interface. As a result, the friction coefficient of MHP5 was higher than that of MHP3.5. As sliding continued, a relatively stable tribo-oxidation film may have gradually formed on the worn surface. In addition, the local depressions generated by hammer peening could partially accommodate wear debris, reducing repeated abrasion by loose particles within the sliding interface. Therefore, the friction coefficient of MHP5 exhibited a gradual decreasing trend during the later stage of the wear process.

MHP1.7 maintains a high friction coefficient of 0.55–0.60, similar to the stable stage of MHP0 but with significantly reduced fluctuation. Low-energy hammering only induces slight plastic deformation in the coating surface, with limited grain refinement and hardness increase, insufficient to notably improve resistance to plowing, and thus cannot reduce the

friction coefficient. However, hammering removes sharp surface protrusions and some casting defects, reducing initial roughness irregularities and improving friction stability.

In comparison, under a low 30 N load, MHP3.5 provides the best optimization of friction behavior, achieving the lowest friction coefficient and excellent stability; MHP5.0 is second, while MHP1.7 only shows some improvement in stability. These results align with the specific wear rate analysis, further confirming that medium-energy hammering significantly enhances the wear resistance and friction reduction performance of coatings under low-load conditions.

3.3.3. Wear Surface Morphology Analysis

Figure 8 shows the three-dimensional surface morphology of CoCrFeMnNi high-entropy alloy coatings treated with different hammering energies after sliding against a SiC pin under a 30 N load for 10 min. MHP0 exhibits pronounced periodic grooves and a relatively low surface height range (−21.37 to 26.72 μm), with small overall height fluctuations. This indicates that under 30 N load, the hard SiC easily penetrated the original low-hardness (~190 HV) coating, displaying typical abrasive wear characteristics (Figure 8a), explaining the severe friction coefficient fluctuations and the highest specific wear rate.

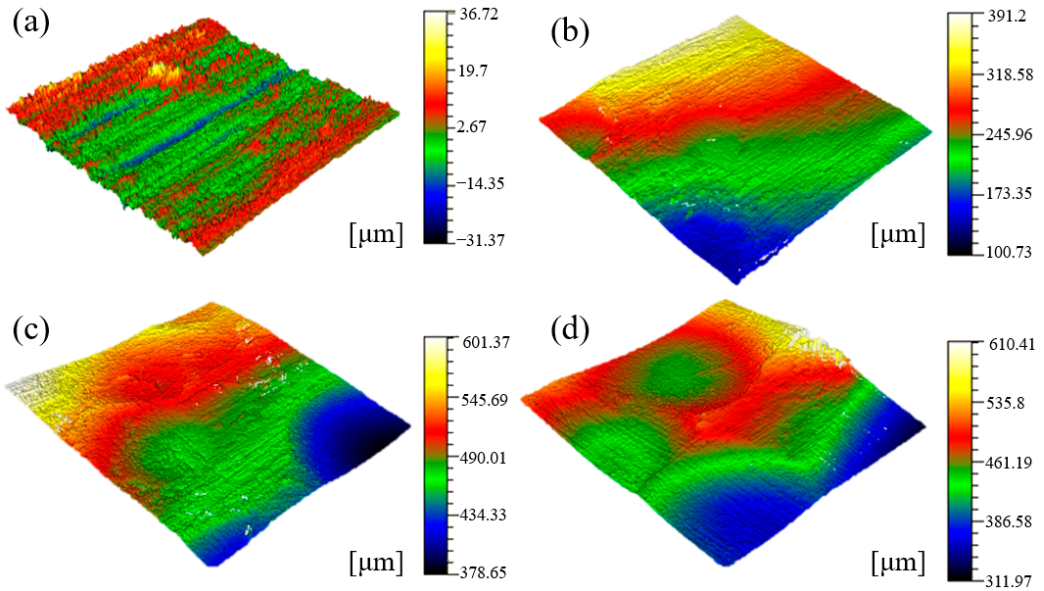


Figure 8. Surface morphology of mechanically hammered coatings after friction and wear under 30 N load: (**a**) MHP0, (**b**) MHP1.7, (**c**) MHP3.5, and (**d**) MHP5.

With increasing hammering energy, the surface morphology changes significantly: MHP1.7 shows weakened grooves and a marked increase in surface height (100.73 to 291.2 μm) (Figure 8b). Although macroscopic undulations from hammering are present, small wear scratches are still observed at the tops, indicating that low-energy strengthening provides limited resistance to plastic deformation. MHP3.5 reaches the maximum surface height (379.65 to 601.37 μm) with local high-point regions (Figure 8c). Despite pronounced macroscopic undulations, the "island-like" high points in actual contact areas are relatively smooth, and grooves are shallower, due to the formation of a 420 HV hard surface layer, significantly enhancing resistance to abrasive cutting, resulting in the lowest friction coefficient and wear amount. MHP5 exhibited a more complex island-like surface morphology with a central depression–protrusion feature, as shown in Figure 8d, and the surface height ranged from 311.97 to 610.41 μm. Although the surface hardness of MHP5 remained significantly higher than that of the untreated coating, it was lower than that of

MHP3.5. Moreover, a more pronounced hardness reduction was observed in the deeper regions, suggesting that the strengthened layer produced by 5 J hammer peening may possess a certain degree of non-uniformity.

At the same time, the friction coefficient of MHP5 was higher than that of MHP3.5. In the high-magnification SEM image shown in Figure 9(d_3), a small number of microcracks, micro-spallation pits, and fine wear debris can also be observed. Based on the combined results of hardness distribution, friction behavior, and local wear morphology, it can be inferred that excessive hammering energy may lead to a non-uniform distribution of plastic strain, defect density, and residual stress within the surface layer. Such heterogeneity may reduce the local deformation compatibility of certain regions and promote a tendency toward local embrittlement under cyclic contact stress. It should be noted that this interpretation is only intended to explain the observed local crack initiation and micro-spallation phenomena during the wear process and does not imply a reduction in the overall fracture toughness of the coating.

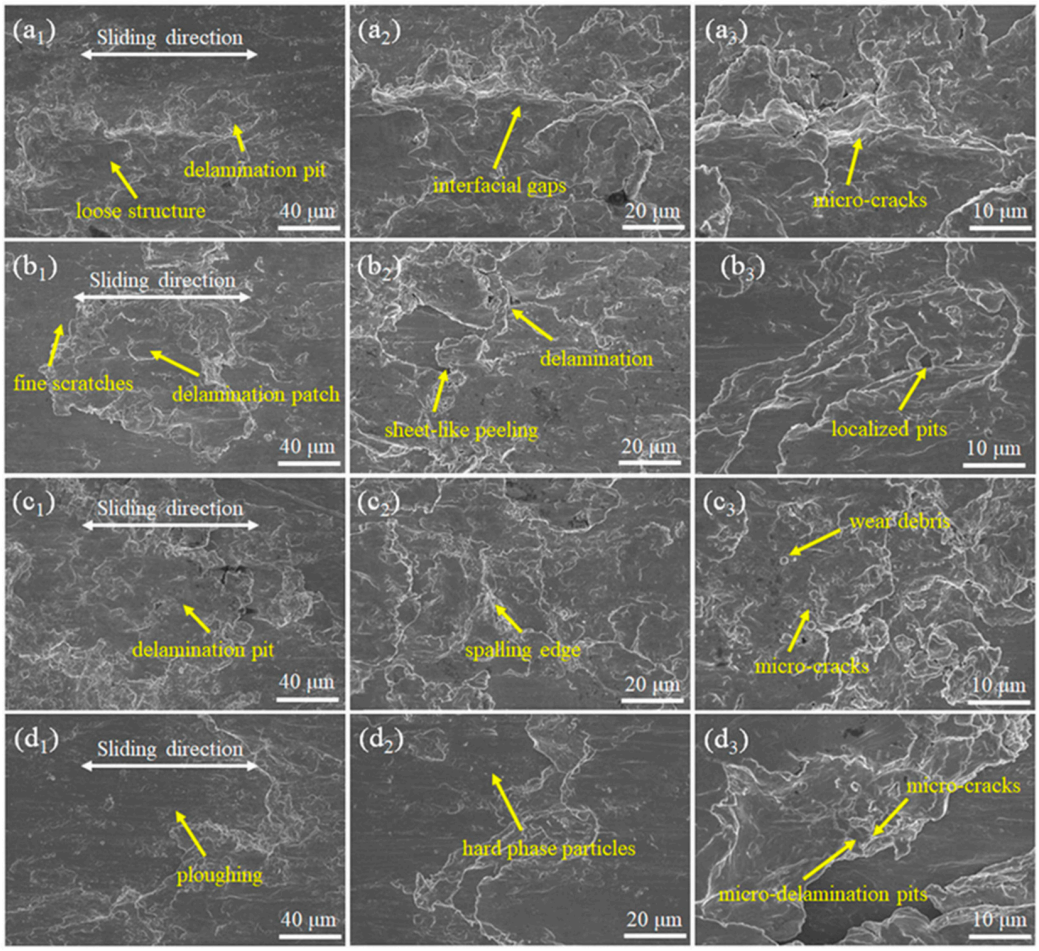


Figure 9. SEM images of wear surfaces of CoCrFeMnNi high-entropy alloy coatings under 30 N load with different hammering energies: (**a_1**–**a_3**) MHP0, (**b_1**–**b_3**) MHP1.7, (**c_1**–**c_3**) MHP3.5, and (**d_1**–**d_3**) MHP5.

In summary, MHP0 mainly undergoes severe abrasive wear. After medium-energy hammer peening, the surface hardness increases stepwise, which is closely related to the impact-induced severe plastic deformation and its corresponding hardening mechanisms, effectively hindering SiC particle penetration and spallation, which is the core reason for the significantly enhanced wear resistance of the coating.

3.3.4. Wear Mechanism Analysis

Figure 9 shows SEM micrographs of CoCrFeMnNi high-entropy alloy coatings treated with different hammering energies after sliding against a SiC pin under a 30 N load. Different magnifications reveal the systematic differences in wear mechanisms among the samples.

The MHP0 sample exhibits obvious damage features under a relatively low 30 N load (Figure 9(a_1–a_3)). The low-magnification image (a_1) shows severe material loss due to the presence of porous structures in the original coating, with significant exfoliation pits distributed across the surface. The medium-magnification image (a_2) further reveals the cause of material failure, showing evident interfacial gaps between molten particles, which act as stress concentration points, leading to rapid crack propagation along layers and eventual delamination. The high-magnification image (a_3) captures micro-details of the worn surface, where microcracks initiate on particle surfaces and penetrate the oxide or delaminated layers, reflecting a combined mechanism of adhesive wear and surface fatigue.

Compared with MHP0, MHP1.7 exhibits different wear morphology (Figure 9(b_1–b_3)). The low-magnification image (b_1) shows uniform fine scratches and localized peeling patches instead of network cracks. The medium-magnification image (b_2) reveals flake delamination and partial layering, while the high-magnification image (b_3) shows local pit formation. These features indicate that low-energy hammer peening altered the wear behavior of the coating surface, with the worn morphology mainly characterized by local delamination, fine scratches, and adhered wear debris. Compared with MHP0, the continuous cracks and large-area spallation observed on the MHP1.7 surface were significantly reduced, indicating that surface hardening improved the coating's resistance to material detachment and abrasive ploughing to a certain extent. Based on the SEM observations, the dominant wear mechanisms of MHP1.7 were identified as delamination wear and mild abrasive wear. In addition, under dry sliding conditions, freshly exposed metallic surfaces and fine wear debris may undergo oxidation, leading to the formation of oxide debris or tribo-oxide films that participate in the interfacial evolution process. Previous studies [27,28] on CoCrFeMnNi high-entropy alloys have reported that oxidation commonly acts as an accompanying mechanism during dry sliding wear. Therefore, oxidation may also have contributed to the wear process of the MHP1.7 sample.

Increasing the hammering energy to MHP3.5, the wear surface (Figure 9(c_1–c_3)) shows distinctive microfeatures. The low-magnification image (c_1) reveals clear exfoliation pits with sharper edges than MHP0, indicating severe fatigue delamination under cyclic high load on the high-hardness surface. The medium-magnification image (c_2) shows layered tearing at the edges of delaminated areas and prominent delamination boundaries, reflecting crack propagation at the coating-substrate interface or within the strengthened layer. The high-magnification image (c_3) reveals numerous wear debris within and around the pits, with microcracks induced by stress concentration. Overall, the wear mechanism of MHP3.5 at 30 N mainly involves a combination of fatigue and adhesive wear. While hammering significantly increases surface hardness, excessive hammering may introduce high residual tensile stress or reduce local toughness, making the material more prone to brittle delamination, with hard debris acting as a "third body" that further aggravates wear.

The wear surface of MHP5 (Figure 9(d_1–d_3)) exhibits distinct features from other samples. The low-magnification image (d_1) shows regular wear tracks mainly consisting of shallow parallel plow grooves along the sliding direction, demonstrating strong cutting resistance of the strengthened layer. The medium-magnification image (d_2) reveals dispersed hard-phase particles on the surface, effectively blocking further plowing by abrasive particles, shifting the wear mechanism from pure abrasive wear to limited mild wear. The high-magnification image (d_3) captures very few micro-exfoliation pits and fine wear debris

at the groove edges and hard-phase interfaces. This indicates that under sustained 30 N contact stress, only extremely superficial fatigue delamination and mild adhesive wear occur. Owing to the grain refinement and surface strengthening effects induced by machine hammer peening (MHP), the wear damage was largely confined to the near-surface region, without extensive material delamination or deep crack propagation. As a result, the coating exhibited enhanced resistance to surface damage.

A comprehensive analysis indicates that the wear mechanisms of the CoCrFeMnNi high-entropy alloy coatings were strongly influenced by the hammering energy and exhibited nonlinear evolution behavior. Under the 30 N load condition, the dominant wear mechanism evolved from adhesive wear and surface fatigue wear in the untreated coating (MHP0) to delamination wear and oxidative wear in MHP1.7, fatigue wear accompanied by slight adhesive wear in MHP3.5, and finally mild abrasive wear together with superficial fatigue spallation in MHP5 as the hammering energy increased. Although the MHP5 sample exhibited relatively mild surface damage and a more intact worn morphology, the worn-surface appearance alone cannot fully represent the overall wear resistance of the coating. When the friction coefficient, specific wear rate, and hardness results are considered together, the MHP3.5 sample exhibited the highest surface hardness, the lowest specific wear rate, and the most stable friction behavior. These results indicate that intermediate hammering energy can achieve an optimal balance between grain refinement, strain hardening, and surface plastic deformation, thereby providing the best overall wear resistance.

To further evaluate the effectiveness of machine hammer peening, the tribological performance obtained in the present study was compared with previously reported results for laser-cladded CoCrFeMnNi coatings and other surface-strengthened alloy systems. Ding et al. [13] reported that the wear resistance of laser-cladded CoCrFeMnNi coatings was strongly influenced by processing-induced microstructural characteristics, while Nagarjuna et al. [16] demonstrated that the wear behavior of CoCrFeMnNi alloys is closely related to subsurface deformation and microstructural evolution during sliding. In addition, previous studies on machine hammer peening and related surface severe plastic deformation treatments have shown that grain refinement, strain hardening, and compressive residual stresses can effectively improve the wear resistance of metallic materials and coatings [20,24,25].

In the present work, the MHP3.5 coating exhibited a surface hardness of approximately 420 HV and achieved a nearly 45% reduction in specific wear rate compared with the untreated coating. Furthermore, the friction coefficient remained relatively stable at approximately 0.40–0.45 during steady-state sliding. This observation is consistent with the findings of Escherová et al. [29], who reported that wear resistance is governed not only by friction coefficient but also by microstructural characteristics, hardness, and wear mechanisms. These results indicate that machine hammer peening can significantly enhance the tribological performance of laser-cladded CoCrFeMnNi coatings. The improvement is mainly attributed to the synergistic effects of surface hardening, grain refinement, and deformation-induced microstructural strengthening. Therefore, the present study provides further evidence that hammering energy is an important process parameter governing the wear performance of laser-cladded high-entropy alloy coatings.

4. Conclusions

(1) Different hammering energies do not alter the phase composition of laser-cladded CoCrFeMnNi high-entropy alloy coatings, which consistently retain a single-phase face-centered cubic (FCC) crystal structure, exhibiting good structural stability. As

hammering energy increases, the surface morphology transitions from discrete hammer pits (MHP1.7) to an "orange-peel" texture (MHP5);

(2) Machine hammer peening significantly increases surface hardness and establishes an ideal hardness gradient. In the surface region (0–300 μm), MHP3.5 exhibits the highest hardness, approximately 420 HV, about 120% higher than the unpeened sample; MHP1.7 and MHP5 show surface hardness increases of about 110% and 95%, respectively. Hardness enhancement exhibits a nonlinear relationship with hammering energy, with medium-energy hammering (3.5 J) providing the optimal strengthening effect;

(3) Specific wear rate tests indicate that under a low 30 N load, medium-energy hammering achieves optimal wear resistance, while excessively high or low energies fail to produce the best low-load wear strengthening. Friction coefficient analysis shows that MHP3.5 optimizes friction behavior most effectively, achieving the lowest friction coefficient and excellent stability; MHP5.0 ranks second, and MHP1.7 shows only some improvement in stability.

Wear mechanism analysis reveals that the dominant wear mechanism evolved progressively with increasing hammering energy under a load of 30 N, changing from adhesive wear and surface fatigue wear in the untreated coating (MHP0), to delamination wear and oxidative wear in MHP1.7, fatigue wear accompanied by slight adhesive wear in MHP3.5, and finally mild abrasive wear together with superficial fatigue spallation in MHP5. Among the investigated conditions, the MHP3.5 sample achieved the most favorable balance between wear-damage suppression and overall wear resistance. The comprehensive results demonstrate that machine hammer peening is an effective post-treatment approach for enhancing the overall performance of CoCrFeMnNi high-entropy alloy coatings. Under the wear condition of a 30 N load, the MHP3.5 sample exhibited the highest surface hardness, the lowest specific wear rate, and the most stable friction behavior among the investigated conditions. These results suggest that intermediate hammering energy is beneficial for achieving a desirable balance among strain hardening, surface deformation tolerance, and potential microstructural refinement, thereby improving the tribological performance of the coating. The findings provide experimental evidence and theoretical support for the application of laser-cladded high-entropy alloy coatings in wear-resistant hydraulic machinery components.

Author Contributions: Conceptualization, X.H.; methodology, R.W.; software, J.H., L.Y. and S.X.; validation, J.H., L.Y., S.X., L.S. and H.W.; formal analysis, R.W.; investigation, R.W.; resources, X.H.; data curation, R.W.; writing—original draft preparation, R.W.; writing—review and editing, J.H., L.Y., S.X., L.S., H.W. and X.H.; visualization, J.H. and L.S.; supervision, X.H. All authors have read and agreed to the published version of the manuscript.

Funding: This research was funded by the National Natural Science Foundation of China, grant number 52575212, and the Large Instruments Open Foundation of Nantong University, grant number KFJN2625.

Data Availability Statement: The original contributions presented in this study are included in the article. Further inquiries can be directed to the corresponding author.

Acknowledgments: The authors would like to appreciate the technical support and material characterization assistance provided by the Analysis and Test Centre of Nantong University.

Conflicts of Interest: The authors declare no conflict of interest.

References

1. Larché, N.; Diler, E.; Thierry, D. Crevice and pitting corrosion of stainless-steel and nickel based alloys in deep sea water. In Proceedings of the NACE CORROSION, Nashville, TN, USA, 24–28 March 2019; Paper No. NACE-2019-13123.
2. Shi, L.; Huo, D.; Lei, Y.; Qu, S.; Chang, X.; Yin, Y. Effect of microstructure on tribocorrosion of FH36 low-temperature steels. *High Temp. Mater. Process.* **2022**, *41*, 328–342. [CrossRef]
3. Singh, R.; Tiwari, S.K.; Mishra, S.K. Cavitation erosion in hydraulic turbine components and mitigation by coatings: Current status and future needs. *J. Mater. Eng. Perform.* **2012**, *21*, 1539–1551. [CrossRef]
4. Mei, Z.; Du, L.; Zhao, X.H. Research on surface treatment technologies of chemical materials. *Chem. Fiber Text. Technol.* **2024**, *53*, 61–63.
5. Liang, Y.; Liao, Z.Y.; Zhang, L.L.; Cai, M.W.; Wei, X.S.; Shen, J. A review on coatings deposited by extreme high-speed laser cladding: Processes, materials, and properties. *Opt. Laser Technol.* **2023**, *164*, 109472. [CrossRef]
6. Cantor, B.; Chang, I.T.H.; Knight, P.; Vincent, A.J.B. Microstructural development in equiatomic multicomponent alloys. *Mater. Sci. Eng. A* **2004**, *375–377*, 213–218. [CrossRef]
7. Yeh, J.W.; Chen, S.K.; Lin, S.J.; Gan, J.Y.; Chin, T.S.; Shun, T.T.; Tsau, C.H.; Chang, S.Y. Nanostructured high-entropy alloys with multiple principal elements: Novel alloy design concepts and outcomes. *Adv. Eng. Mater.* **2004**, *6*, 299–303. [CrossRef]
8. Zhang, Y.; Zuo, T.T.; Tang, Z.; Gao, M.C.; Dahmen, K.A.; Liaw, P.K.; Lu, Z.P. Microstructures and properties of high-entropy alloys. *Prog. Mater. Sci.* **2014**, *61*, 1–93. [CrossRef]
9. Miracle, D.B.; Senkov, O.N. A critical review of high entropy alloys and related concepts. *Acta Mater.* **2017**, *122*, 448–511. [CrossRef]
10. Arif, Z.U.; Khalid, M.Y.; Rehman, E.U.; Ullah, S.; Atif, M.; Tariq, A. A review on laser cladding of high-entropy alloys, their recent trends and potential applications. *J. Manuf. Process.* **2021**, *68*, 225–273. [CrossRef]
11. Xiang, K.; Chen, L.Y.; Chai, L.; Guo, N.; Wang, H. Microstructural characteristics and properties of CoCrFeNiNbx high-entropy alloy coatings on pure titanium substrate by pulsed laser cladding. *Appl. Surf. Sci.* **2020**, *517*, 146214. [CrossRef]
12. Ma, G.; Zhao, Y.; Cui, H.; Song, X.; Wang, M.; Lee, K.; Gao, X.; Song, Q.; Wang, C. Addition Al and/or Ti induced modifications of microstructures, mechanical properties, and corrosion properties in CoCrFeNi high-entropy alloy coatings. *Acta Metall. Sin. (Engl. Lett.)* **2021**, *34*, 1087–1102. [CrossRef]
13. Ding, C.C.; Liu, Y.; Ni, H.J.; Wang, X.; Wang, H. Effects of laser energy density on microstructure, texture and tribological property of CoCrFeMnNi high entropy alloy coatings fabricated by laser cladding. *Surf. Interfaces* **2025**, *61*, 106107. [CrossRef]
14. Melia, M.A.; Carroll, J.D.; Whetten, S.R.; Esmaeely, S.N.; Locke, J.; White, E.; Anderson, I.; Chandross, M.; Michael, J.R.; Argibay, N.; et al. Mechanical and corrosion properties of additively manufactured CoCrFeMnNi high entropy alloy. *Addit. Manuf.* **2019**, *29*, 100833. [CrossRef]
15. Gu, G.H.; Kim, R.E.; Lee, J.; Kim, H.S. Tailoring microstructure with spatial heterogeneity in CoCrFeMnNi high-entropy alloy via laser surface relaxation. *Mater. Sci. Eng. A* **2022**, *852*, 143720. [CrossRef]
16. Han, Y.; Li, H.; Feng, H.; Li, K.; Tian, Y.; Jiang, Z. Enhancing the strength and ductility of CoCrFeMnNi high-entropy alloy by nitrogen addition. *Mater. Sci. Eng. A* **2020**, *789*, 139587. [CrossRef]
17. Joseph, J.; Haghdadi, N.; Shamlaye, K.; Hodgson, P.; Barnett, M.; Fabijanic, D. The sliding wear behaviour of CoCrFeMnNi and AlxCoCrFeNi high entropy alloys at elevated temperatures. *Wear* **2019**, *428–429*, 32–44. [CrossRef]
18. Nagarjuna, C.; You, H.J.; Ahn, S.; Song, J.W.; Jeong, K.Y.; Madavali, B.; Song, G.; Na, Y.S.; Won, J.W.; Kim, H.S. Worn surface and subsurface layer structure formation behavior on wear mechanism of CoCrFeMnNi high entropy alloy in different sliding conditions. *Appl. Surf. Sci.* **2021**, *549*, 149202. [CrossRef]
19. Fan, X.; Qu, R.; Zhang, Z. Relation between strength and hardness of high-entropy alloys. *Acta Metall. Sin. (Engl. Lett.)* **2021**, *34*, 1461–1482. [CrossRef]
20. Schulze, V.; Bleicher, F.; Groche, P.; Guo, Y.B.; Pyun, Y.S. Surface modification by machine hammer peening and burnishing. *CIRP Ann.* **2016**, *65*, 809–832. [CrossRef]
21. Dadgar, M.; Gräfe, S.; Müller, M.; Herrig, T.; Bergs, T. Surface integrity of additively manufactured workpieces after machine hammer peening. *Procedia CIRP* **2024**, *123*, 161–166. [CrossRef]
22. Liu, Q.; Chen, S.; Xu, X.; Jin, S.; Li, Y.; Wang, Y.; Shen, B. Multi-objective optimization of the subsurface residual stress field of TC4 alloy in machine hammer peening. *J. Manuf. Process.* **2023**, *104*, 98–107. [CrossRef]
23. Lin, X.H.; Huang, H.B.; Zhou, C.S.; Liu, J.C.; Saleh, M.; Wang, Z.Z. Research on surface modification of anodized aluminum alloy using piezoelectric machine hammer peening. *Int. J. Adv. Manuf. Technol.* **2019**, *104*, 1211–1219. [CrossRef]
24. Rausch, S.; Wiederkehr, P.; Biermann, D.; Zabel, A.; Selvadurai, U.; Hagen, L.; Tillmann, W. Influence of machine hammer peening on the tribological behavior and the residual stresses of wear resistant thermally sprayed coatings. *Procedia CIRP* **2016**, *45*, 275–278. [CrossRef]

25. Rausch, S.; Wiederkehr, P.; Biermann, D.; Zabel, A.; Selvadurai, U.; Hagen, L.; Tillmann, W. Grinding- and robotic hammer peening-induced modifications in the near-surface regions of laser-cladded Inconel 718 coatings. *Surf. Coat. Technol.* **2024**, *489*, 131130.
26. Wang, B. Study on the Effects of Mechanical Hammer Peening and Annealing Treatment on the Surface Properties of TC4 Titanium Alloy. Master's Thesis, Wuhan University of Science and Technology, Wuhan, China, 2021.
27. Wang, Y.; Li, D.; Yang, J.; Jin, J.; Zhang, M.; Wang, X.; Li, B.; Hu, Z.; Gong, P. Effect of Grain Size on the Tribological Behavior of CoCrFeMnNi High Entropy Alloy. *Materials* **2023**, *16*, 1714. [CrossRef] [PubMed]
28. Li, C.; Ma, Z.; Tong, S.; Liu, J.; Zhang, W.; Shen, G.; Wang, S.; Zhao, H.; Ren, L. Mechanical-thermal coupling fatigue failure of CoCrFeMnNi high entropy alloy. *J. Mater. Res. Technol.* **2024**, *30*, 3430–3437. [CrossRef]
29. Escherova, J.; Krbata, M.; Krizan, D.; Kohutiar, M.; Trembach, B.; Kluciar, P.; Beronska, N.; Nagy, S.; Commenda, C. Comparison of wear resistance of lean medium Mn AHSS after Q&P heat treatment. *Metals* **2026**, *16*, 362. [CrossRef]

Disclaimer/Publisher's Note: The statements, opinions and data contained in all publications are solely those of the individual author(s) and contributor(s) and not of MDPI and/or the editor(s). MDPI and/or the editor(s) disclaim responsibility for any injury to people or property resulting from any ideas, methods, instructions or products referred to in the content.